The Upscale Turbulent Cascade

Shear Layers, Cyclones and Gas Giant Bands

W. R. Peltier[1] and G. R. Stuhne[1,2]

[1]*Department of Physics, University of Toronto, Toronto, Ontario, Canada*
[2]*Scripps Institution of Oceanography (PORD Division), University of California, San Diego, La Jolla, CA, USA*

The upscale cascade of kinetic energy which characterizes the evolution of turbulent flows that are restricted to two spatial dimensions is mediated by the vortex-pairing interaction. In randomly initialized flows on the *f*-plane, this interaction coarsens the initial vorticity distribution by causing like-signed vortices to amalgamate and thereby leads to the creation of coherent vortical structures of ever-increasing spatial scale. In the sequence of analyses discussed herein, we analyse a series of problems of interest from an atmospheric dynamics perspective in which, in spite of their intrinsically three (or 2.5) dimensionality, the vortex-pairing interaction is nevertheless active and has important phenomenological consequences. These problems include the "classical" problems of parallel shear and baroclinic instability as well as the somewhat more exotic problem of vortex dynamics in shallow water flow on the surface of the sphere.

A. INTRODUCTION

Ever since the work of Fjortoft (1953; see also Salmon, 1998) it has been well understood that the inviscid flow of a classical fluid (whether liquid or gas), if confined to two space dimensions, is constrained to evolve such that kinetic energy "cascades" from smaller to larger spatial scales. This behaviour is a simple mathematical consequence of the joint constraints of kinetic energy and enstrophy (mean-square vorticity) conservation. Charney (1971) extended Fjortoft's result to the case of three-dimensional quasi-geostrophic flow. Although the validity of this result has been contradicted by both early numerical model results (e.g. Barros and Winn-Nielsen, 1974; Hua and Haidvogel, 1986) and by the analysis of atmospheric observations (e.g. see the analysis FGGE III data by Lambert, 1981), more results appear to confirm it.

In spite of the fact that vorticity is clearly not conserved in three-dimensional flows, in consequence of the action of the processes of vortex stretching and tilting through which vorticity may be generated or destroyed, there is nevertheless considerable interest in understanding the extent to which the fundamental interaction that supports the upscale cascade in two space dimensions may still manifest itself to some degree in three-dimensional reality. In two-dimensional flows on the *f*-plane (e.g. McWilliams, 1984; Maltrud and Vallis, 1991), this fundamental interaction is clearly seen to involve the "pairing" of vortices of like sign so as to produce coherent vortical structures of ever-increasing spatial scale. Since three-dimensional turbulent flows are clearly not constrained in general by this interaction and so may (and of course do) transfer kinetic energy downscale (Kolmogorov, 1941), it is an interesting question as to whether and in what circumstances there may nevertheless remain vestiges of the pairing interaction in three-dimensional flows. An equally interesting question, if such vestigal effects of the pairing interaction do remain in three-dimensional flows, concerns the processes that conspire to limit their spatiotemporal range of influence.

In this chapter our intention is to describe an exploration of these questions in which three different flows are analysed which have distinctly different geometries and physical properties but which share the characteristic that the pairing interaction exerts significant control on flow evolution, at least initially, even though the flows are intrinsically three dimensional (or at least 2.5 dimensional). In each of these three cases it will be argued that the vortex-merging interaction exerts intense though ephemeral control on flow evolution. Since our purpose herein is to compare

the hydrodynamic phenomenology that occurs in these three distinctly different circumstances and since the analyses that have been performed of each flow geometry are each fairly complex in themselves, space will allow only the most cursory presentation of the methodology employed and results obtained in each case.

As implied in the title of this chapter, we will begin with a discussion of the simplest circumstance in which the pairing interaction occurs, namely that of a sheared parallel flow containing an "inflection point" in the velocity profile. The classical problem of the baroclinic instability of a zonal flow that is initially in thermal wind balance is considered subsequently, analysis of which suggests the existence of a route to deep development that does not begin on the Charney–Eady branch of unstable modes but rather with a subsynoptic-scale instability through which finite-amplitude vortices are engendered and which, through the pairing interaction, subsequently produces a deep energetic disturbance of wavelength that is still significantly less than that of the most unstable Charney–Eady wave. Finally, we will consider the spherical problem of vortex merging in which, through the Rossby-wave arrest of the upscale cascade (Rhines, 1975), a banded zonal velocity profile may develop that very well mimics the observed zonal velocity patterns visible on the discs of the Gas Giant planets Jupiter, Saturn, Neptune and Uranus. In the latter context the focus will be upon the mechanism whereby the upscale cascade is arrested and the way in which this determines the sign of the equatorial jet that emerges in the limit of long time. Conclusions based upon this intercomparison of the three model problems are offered in the final section.

B. PAIRING IN UNSTRATIFIED SHEAR FLOW

If confined so as to evolve in two space dimensions, an unstratified flow with vorticity $\omega = \nabla \times \mathbf{u}$, with $\mathbf{u}$ the velocity field, will advance in time so as to satisy the system

$$\frac{\partial \omega}{\partial t} = \frac{\partial \omega}{\partial x}\frac{\partial \Psi}{\partial z} - \frac{\partial \omega}{\partial z}\frac{\partial \Psi}{\partial x} + \frac{1}{R_e}\nabla^2 \omega \qquad (1a)$$

$$\nabla^2 \Psi = -\omega \qquad (1b)$$

in which Ψ is the stream function such that $u = -\partial\Psi/\partial z$, $w = \partial\Psi/\partial x$, and $\mathrm{Re} = U_o h/\nu$ is the Reynolds number with U_o and h characteristic velocity and length scales respectively and ν the kinematic viscosity. Suppose we assume initial conditions such that $\mathbf{u} = U(z) = U_o \tanh(z/h)$ so that nondimensional $\omega(z) = 1/\cosh^2 z$ initially. If R_e is $\gtrsim 50$, then the initially parallel flow is Kelvin–Helmholtz (K-H) unstable and will evolve in the presence of weak noise so as to generate a train of like-signed vortices in which the fundamental wavelength λ_f is approximately seven times the initial depth of the shear layer. This length scale is of course precisely predictable on the basis of the solution of the associated two-point boundary-value problem for linear stability. Even in the presence of stable density stratification (Smyth and Peltier, 1990), the primary instability of the initial parallel flow is inevitably two dimensional unless the density stratification is extreme. Figure 1 illustrates the evolution of an unstratified flow according to equations (1) computed in a rectangular domain of length $2\lambda_f$ in which the spatial boundary conditions are periodic in x and impermeable at $z = \pm H$, with $H >> h$ so that the horizontal boundaries exert no control on flow development. Inspection of Fig. 1 demonstrates that once the initial K-H instability saturates the two like-signed vortices in the domain thereafter begin to orbit one-another and eventually fully merge, a process which ends in the creation of a single vortex of double the length scale of the initial train of K-H waves. This is the fundamental interaction that supports the upscale cascade of energy in two-dimensional turbulence. If we were to sufficiently increase both the horizontal and vertical scales of the domain, the merger process would continue unimpeded (Smyth and Peltier, 1993), leading to the creation of vortical structures of ever-increasing scale.

The pairing interaction itself may be very simply understood on the basis of a linear stability analysis of the finite-amplitude vorticity distribution that exists at the moment that the initial K-H instability saturates. Approximating this vorticity distribution by the analytical Stuart (1967) solution to the time-independent Euler equations, we have the solution for the stream function Ψ as:

$$\Psi = -\frac{(1-e)^2}{1-e^2}\log[\cosh(z - h/2) + e\cos x] \qquad (2a)$$

which corresponds to the vorticity distribution

$$\omega = \frac{1-e}{\cosh(z - h/2) + e\cos x} \qquad (2b)$$

in which e is the ellipticity parameter of the Stuart model. Figure 2 shows ω and Ψ for the Stuart solution for several values of the ellipticity parameter. Initial analyses of the stability of the Stuart solution were presented by Kelly (1967) for small amplitude and later by Pierrehumbert and Widnall (1982) for arbitrary amplitude, but at overly low spatial resolution, and by Klaassen and Peltier (1989) at spatial resolution sufficiently high to capture the stability characteristics accurately. Potylitsin and Peltier (1998, 1999) have more recently employed the same model to represent a columnar vortex in a rotating

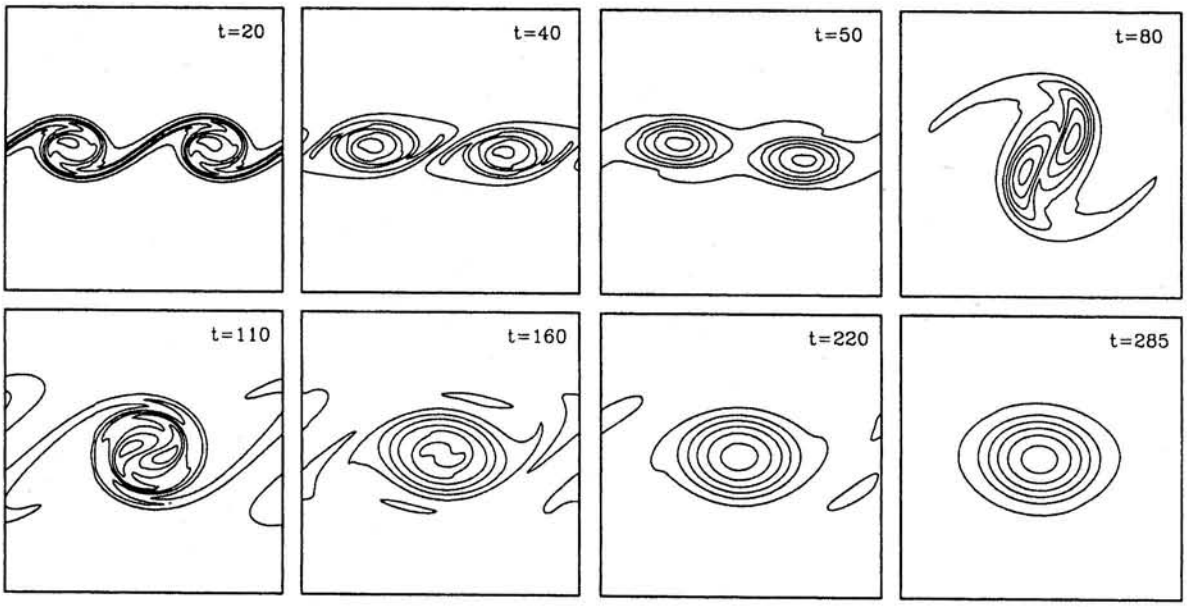

FIGURE 1 The evolution of the vorticity field in two-dimensional homogeneous fluid for a sequence of eight times, beginning with the time of saturation of the primary Kelvin–Helmholtz wave. The horizontal dimension of the domain in which the DNS integration is performed is twice the wavelength λ_f of the fastest growing linear instability. In the limit of long time the vorticity field engendered by the vortex pairing instability consists of a train of vortices with twice the wavelength of the initial train of K-H waves.

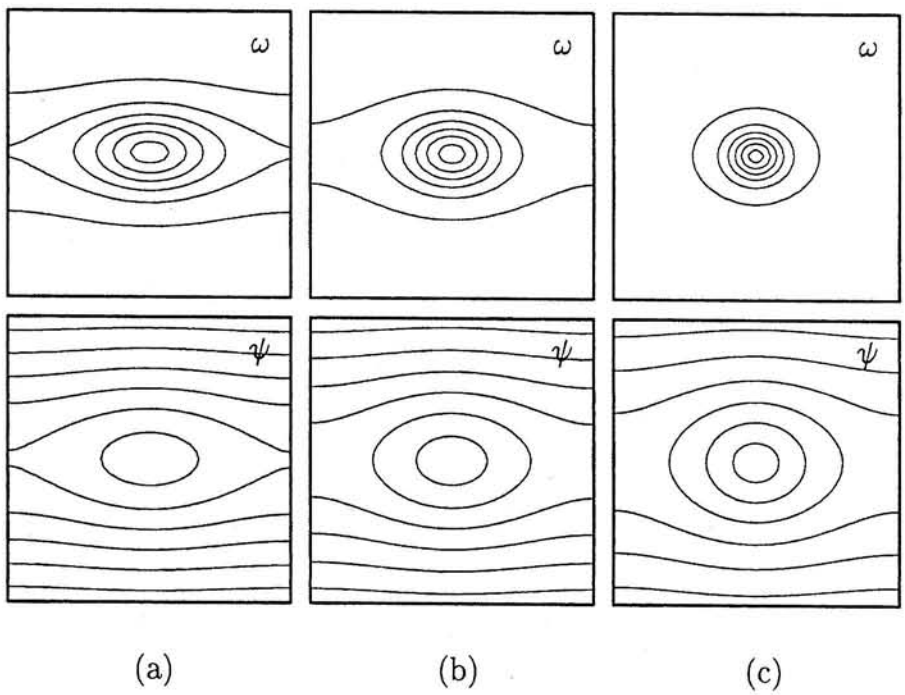

FIGURE 2 Three examples of the vorticity and stream-function fields for the steady Stuart (1967) solution of the Euler equations. In (a); (b) and (c) the values of the ellipticity parameter of the Stuart model are respectively $e = 0.33$ (highly elliptical vortex), $e = 0.5$ (slightly elliptical vortex) and $e = 0.75$ (almost circular vortex).

environment in their investigation of the destabilizing influence of rotation upon upright anticyclones.

The problem of determining the linear stability of a spatially periodic flow such as that represented by equations (2) is a problem in Floquet theory. If we represent the velocity field u_i by the superposition of the two-dimensional Stuart solution, denoted by $\tilde{u}_i(x, z)$ and a perturbation $u_i'(x, y, z, t)$ as:

$$u_i(x, y, z, t) = U_o\tilde{u}_i(x, z, t)(1 - \delta_{i2}) + U_o u_i'(x, y, z, t) \quad (3)$$

then Floquet theory dictates that the Navier–Stokes equation for the solution u_i', with u_i' assumed small, should take the form:

$$u_i'(x, y, z, t) = \hat{u}_i(x, z, t) \exp[\mathrm{i}(bx + dy)] \quad (4)$$

in which $\hat{u}_i$, in general, is a complex function that is periodic in x with fundamental wavelength λ_f fixed to that of the Stuart solution. Since the Stuart solution is precisely steady we may write

$$\hat{u}_i(x, z, t) = u_i^\dagger(x, z)e^{st} \quad (5)$$

with $s = \sigma + i\omega$ the complex eigenvalue of the resulting stability problem. Substituting (3), (4) and (5) into the linearized Boussinesq equations these become:

$$su_x^\dagger + \tilde{u}_x(\partial_x + ib)u_x^\dagger + \tilde{u}_z\partial_z u_x^\dagger + (\partial_x \tilde{u}_x)u_x^\dagger + (\partial_z \tilde{u}_x)\, u_z^\dagger = -(\partial_x + ib)p^\dagger + \frac{1}{R_e} L_2 u_x^\dagger \quad (6a)$$

$$su_y^\dagger + \tilde{u}_x(\partial_x + ib)u_y^\dagger + \tilde{u}_z\partial_z u_y^\dagger = -idp^\dagger + \frac{1}{R_e} L_2 u_y^\dagger \quad (6b)$$

$$su_z^\dagger + \tilde{u}_x(\partial_x + ib)u_z^\dagger + \tilde{u}_z\partial_z u_z^\dagger + (\partial_x \tilde{u}_z)u_x^\dagger + (\partial_z \tilde{u}_z)\, u_z^\dagger = -\partial_z p^\dagger + \frac{1}{R_e} L_2 u_z^\dagger \quad (6c)$$

$$(\partial_x + ib)u_x^\dagger + idu_y^\dagger + \partial_z u_z^\dagger = 0 \quad (6d)$$

with the operator $L_2 = (\partial_x + ib)^2 + \partial_z^2 - d^2$. Since the pairing interaction involves a two-dimensional instability of a two-dimensional flow we may take $d = u_y^\dagger \equiv 0$ so that equation (6b) is redundant and the stability of the Stuart solution will be determined by the simultaneous solution of (6a), (6c) and (6d) with unknowns $u_x^\dagger$, $u_z^\dagger$ and $p^\dagger$, a system with eigenvalue $s = \sigma + i\omega$. Since we may obtain a diagnostic equation for $p^\dagger$ such that

$$L_2 p^\dagger = -2[(\partial_x\tilde{u}_x)(\partial_x + ib)u_x^\dagger + (\partial_z\tilde{u}_z)\partial_z u_z^\dagger + (\partial_x \tilde{u}_z)\partial_z u_x^\dagger + (\partial_z\tilde{u}_z)(\partial_x + ib)u_x^\dagger] \quad (7)$$

$p^\dagger$ is determined by $u_x^\dagger$ and $u_z^\dagger$, for which we may seek solutions in the form of Galerkin expansions as:

$$u_x^\dagger = \sum_{\lambda=-\infty}^{+\infty} \sum_{\nu=0}^{\infty} a_{\lambda\nu}\, e^{i\alpha(2\pi/\lambda)x} \cos\frac{\nu\pi z}{H} \quad (8a)$$

$$u_z^\dagger = \sum_{\alpha=-\infty}^{+\infty} \sum_{\nu=0}^{\infty} b_{\lambda\nu}\, e^{i\alpha(2\pi/\lambda)x} \sin\frac{\nu\pi z}{H} \quad (8b)$$

Upon substitution of (8) into (6) and computation of the inner product of each of equations (6) with the complex conjugates of each of the elements in the Galerkin basis employed in the expansions (8), we obtain the algebraic system:

$$s\, a_{\kappa\mu} = \left(I^{(1)}_{\kappa\mu\alpha\nu} + \frac{A\alpha\nu}{R_e}\delta_{\kappa\alpha}\delta_{\mu\nu}\right) a_{\alpha\nu} + I^{(2)}_{\kappa\mu\alpha\nu} b_{\alpha\nu} \quad (9a)$$

$$s\, b_{\kappa\mu} = I^{(3)}_{\kappa\mu\alpha\nu} + \left(I^{(4)}_{\kappa\mu\alpha\nu} + \frac{A\alpha\nu}{R_e}\delta_{\kappa\alpha}\delta_{\mu\nu}\right) b_{\alpha\nu} \quad (9b)$$

with $A_{\alpha\nu} = B_\alpha^2$, $B_\alpha = \alpha(2\pi/\lambda_f) + b$. By concatenating the coefficients $a_{\kappa\mu}$ and $b_{\kappa\mu}$ so as to form a single subscripted quantity, it will be clear that (9) constitutes a standard matrix eigenvalue problem. The four-subscripted arrays $I^{(1,2,3,4)}_{\kappa\mu\alpha\nu}$ consist of projections of the nonlinear two-dimensional fields onto the Galerkin basis. By appropriate truncation of the Galerkin expansions (8), the algebraic eigenvalue problem (9) is reduced to one of finite dimension and we may compute the eigenvalue s as a function of the Floquet exponent b which describes the wavenumber of the modulation in the x-direction (see (4)) and which is clearly restricted such that $b \leqslant 1$.

Direct calculation shows that the eigenvalues of (9) are such that $\omega \equiv 0$. Figure 3 then shows growth rate σ determined by solving (9) as a function of b for two different truncation schemes, respectively labelled $\beta = 0$ and $\beta = 1/2$. These are:

$$2\,|\,\alpha\,| + \nu \leqslant N \quad (\beta = 0) \quad (10a)$$

$$2\,|\,\alpha + \frac{1}{2}\,| + \nu \leqslant N \quad (\beta = 1\backslash 2) \quad (10b)$$

Inspection of the growth rate spectrum for these two schemes shown in Fig. 3, for the sequence $N = 15, 19, 23$, demonstrates that there are two branches of the modal spectrum, denoted respectively by the solid and dashed lines. In both branches the maximum growth rate occurs at $b = 1/2$, signifying that the fastest-growing instabilities are occurring at the wavelength of the first spatial subharmonic of the initial K-H instability. The eigenfunctions of these two fastest-growing modes are illustrated in Fig. 4 in terms of a superposition of the stream function of the Stuart basic state together with the growing perturbation which is assumed to have an amplitude equal to 1/4 the maximum vorticity. Inspection of these

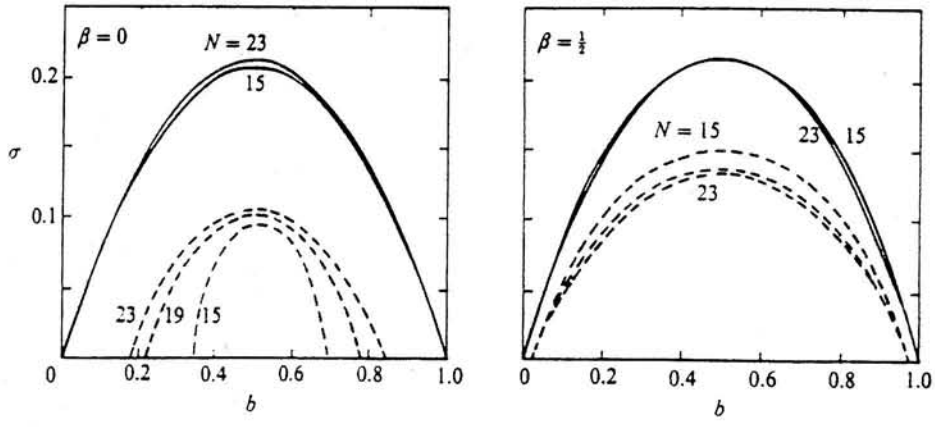

FIGURE 3 Growth rate spectra for the modes of instability of the Stuart solution with $e = 0.5$ as a function of the Floquet parameter b. Results are show for the two different truncation schemes labelled $\beta = 0$ and $\beta = \frac{1}{2}$ which are defined in the text. Results are also shown for three different truncation levels $N = 15$, $N = 19$, and $N = 23$.

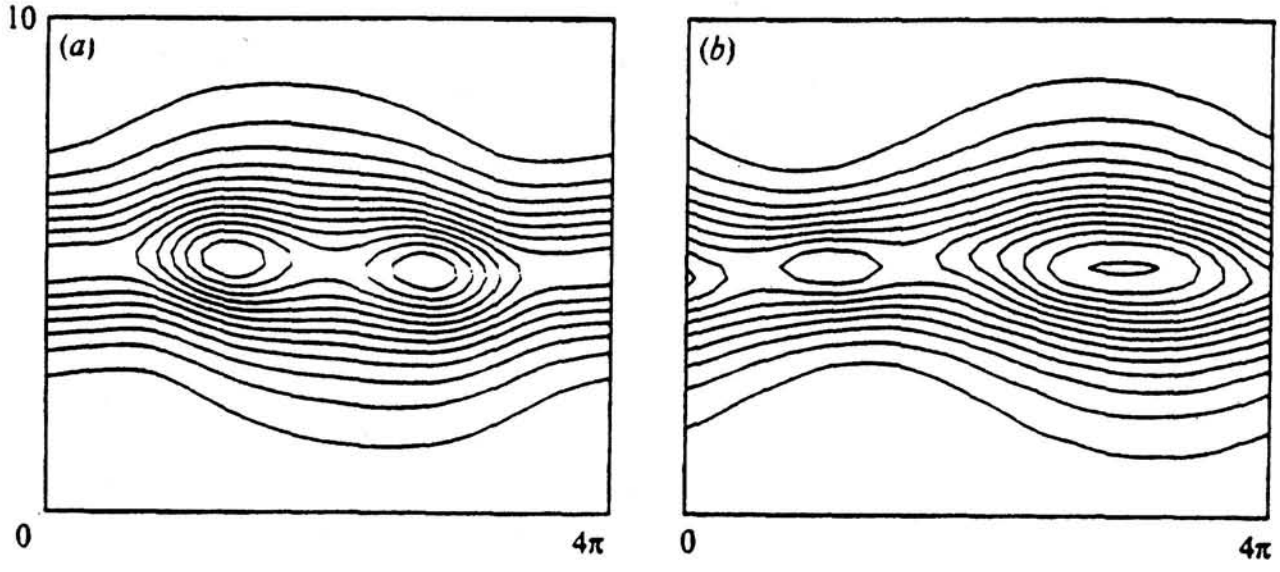

FIGURE 4 Structures of the fastest-growing (subharmonic) instabilities of the Stuart solution for both the orbital-merging mode (a) and for the "draining" mode (b) discussed in the text.

structures will show that the fastest-growing instability at $b = \frac{1}{2}$ shown in (a) corresponds to the first stage of the vortex amalgamation process illustrated previously in Fig. 1. This is the pairing interaction that involves orbital merger. The subdominant second mode at $b = \frac{1}{2}$, whose eigenfunction has been employed to produce the result shown in (b), corresponds conversely, to an interaction in which one vortex grows at the expense of the other by a non-orbital "draining" interaction.

Even in simple two-dimensional shear flows, therefore, the upscale cascade of energy that is mediated by vortex merger, may occur via at least two fundamentally different processes. Furthermore, the bandwidth (in the *Floquet parameter* b) of the merging instabilities is broad, so that the theory explains not only the primary two-vortex interaction but also the more exotic mergers involving $3 \rightarrow 1$ and $3 \rightarrow 2$ interactions that are also observed to occur in laboratory flows, albeit with significantly lower probability (see Klaassen and Peltier 1989 for more detailed discussion). However, when such parallel flows are allowed to access the third space coordinate, the subharmonic pairing interaction must eventually compete with a broad spectrum of fully three-dimensional instabilities for control of flow evolution. These more complex mechanisms may occur on shorter timescales than the pairing interaction and

inhibit it completely. Detailed discussions of these mechanisms will be found in Klaassen and Peltier (1985, 1991), Smyth and Peltier (1991, 1994), Potylitsin and Peltier (1998, 1999), and Caulfield and Peltier (1994, 2000). In the next section we will focus upon the mechanics involved in the baroclinic instability process itself and find further evidence of the importance in fully three-dimensional stratified rotating flow of the action of pairing.

C. PAIRING IN ROTATING STRATIFIED FLOW: SUBSYNOPTIC BAROCLINIC INSTABILITY

Of all of the hydrodynamic interactions that have been studied in the context of our continuing attempts to understand the dynamics of the atmosphere, it is unlikely that any have attracted the same degree of attention as has the baroclinic instability process. Here we will describe a series of results recently obtained in the course of an investigation of the issue of the origins of subsynoptic scale instability (see Yamasaki and Peltier, 2001a,b, for a much more detailed analysis than space will allow herein). Figure 5d–f illustrates the properties of a zonal mean state determined on the basis of Reanalysis Project data from the entrance of the Pacific storm track in winter, while Fig. 5a–c shows the same characterizations of the mean state for an analytical model designed so as to adequately mimic the observations. A notable property of both the observations and the analytical model of them is that there exists a weak horizontal gradient of potential vorticity in the cross-front direction.

Figure 5 shows the results obtained by analysing the linear stability of this two-dimensional basic state to three-dimensional perturbations using exactly the same Galerkin methodology employed in the analysis of the two-dimensional pairing interaction described in the last section. In Fig. 6a,b the modes of instability are characterized respectively by their growth rate and phase speed as a function of the modal wavenumber in the zonal direction parallel to the mean flow. Focusing first on the growth rate spectrum in Fig. 6a, we note that there appears to exist two distinct modal branches. The first, with maximum growth rate at a wavelength near 4000 km, clearly corresponds to the classical Charney–Eady mode. The second modal branch appears to have most rapid growth at a wavelength that is considerably shorter, near 1000 km, although, as the truncation level in the Galerkin representation of the perturbation is increased, there is no evidence of a short-wavelength cutoff for the modes in this branch and the convergence as a function of truncation level is slow. Also shown in Fig. 6a as open circles, with or without an interior "×", are growth rates determined on the basis of DNS using a nonlinear, nonhydrostatic, anelastic model to describe the evolution of the unstable mean state shown in Fig. 5. The growth rates delivered by the nonlinear model, using a "no-noise" initialization procedure (see Yamasaki and Peltier, 2000a, for discussion), are very similar in magnitude but not identical to those delivered by the Galerkin-based analyses of linear stability. Inspection of the phase speed spectra shown in Fig. 6B demonstrates that convergence in this regard is excellent at all wavelengths.

Figure 7 presents the structure of the subsynoptic normal mode determined on the basis of the DNS solution of the initial-value problem in a domain of zonal length λ_f = 1000 km using the complete nonlinear anelastic model. It will be noted that this structure consists of a boundary-trapped disturbance rather than of a deep troposphere filling structure as is characteristic of the conventional synoptic scale Charney-Eady mode. Detailed diagnostic analysis of the energy conversions that are responsible for the growth of the subsynoptic scale structure, perturbation kinetic energy and growth rate time series for which are shown in Figs 8a and 8b respectively, demonstrates that the mode is supported by the baroclinic instability process. The level of perturbation kinetic energy at which this mode saturates, shown in Fig. 8a, however, is clearly rather low, sufficiently low that if no further process were available whereby it might continue to amplify, one could not reasonably expect it to be physically important. In Fig. 9, however, we show a sequence of planform views of the surface potential temperature illustrating the further evolution of this structure that occurs when the zonal length of the domain is simply doubled to $2\lambda_f$. Kinetic energy and growth rate time series from this simulation are shown in Figs 8c and 8d respectively. Evident by inspection of both Figs 8c and 9 is the fact that in the longer zonal domain, the weak subsynoptic scale cyclonic structures undergo a pairing instability after the initial shallow instability saturates, in close analogy with the temporal evolution of the K-H instability discussed in the last section.

After pairing is complete, apparently through a "draining" interaction rather than through orbital merger, the baroclinic disturbance has deepened so as to fill the troposphere and its energy has increased by almost two orders of magnitude, as evidenced by Fig. 8c. The deep structure that develops subsequent to pairing is illustrated in Fig. 10 a,b,c through the zonal average of the squared meridional velocity, the planform of vertically averaged meridional velocity at the surface and a zonal/height cross-section of the same field meridionally averaged. Although this structure is

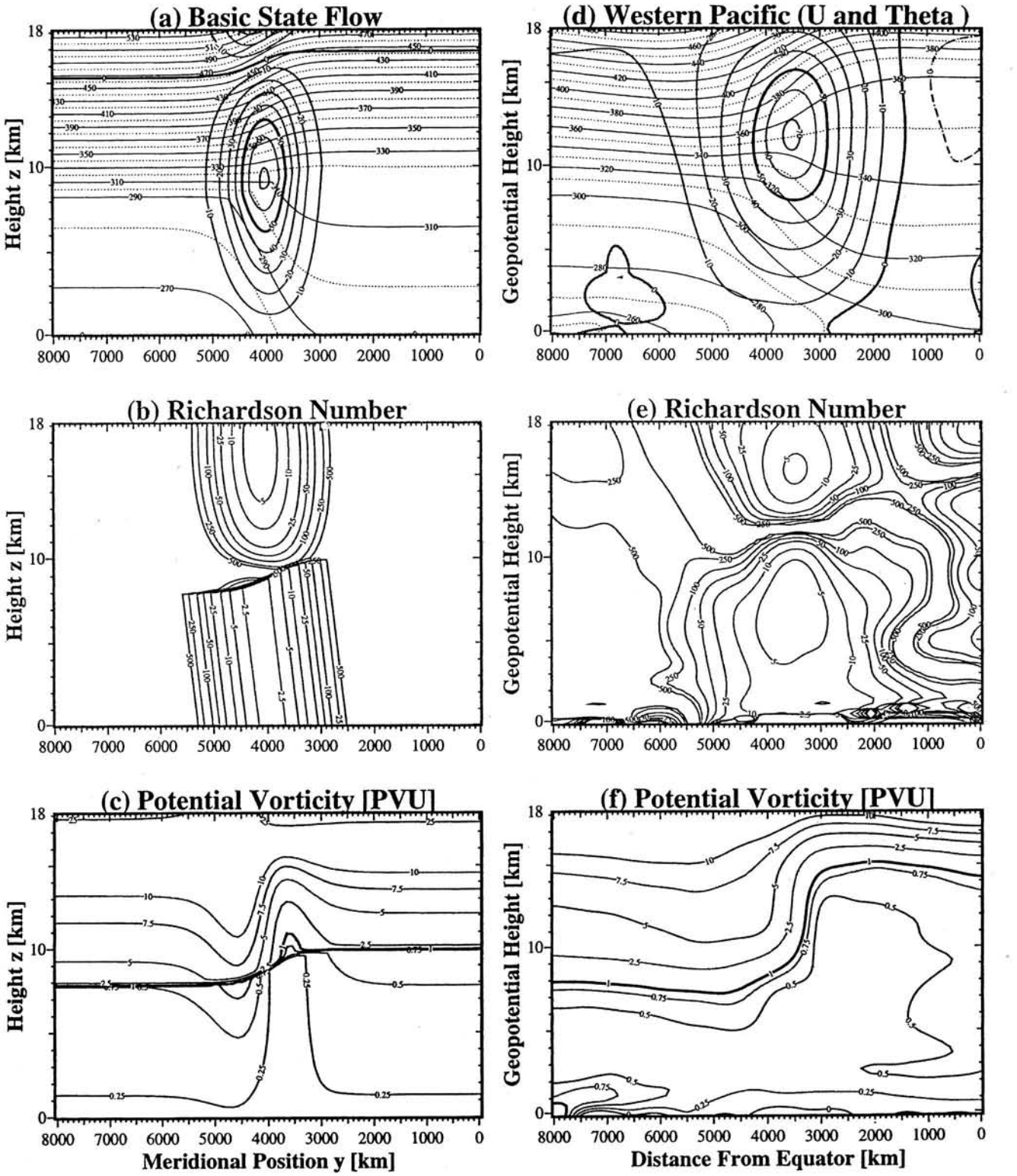

FIGURE 5 Meridional cross-sections of the zonal flow observed at the entrance to the Pacific storm track based upon reanalysis project data expressed in terms of: (d) zonal velocity (u) and potential temperature (θ); (e) Richardson number and (f) potential vorticity. The same fields are shown in (a)–(c) for the analytical model of Yamasaki and Peltier (2000a).

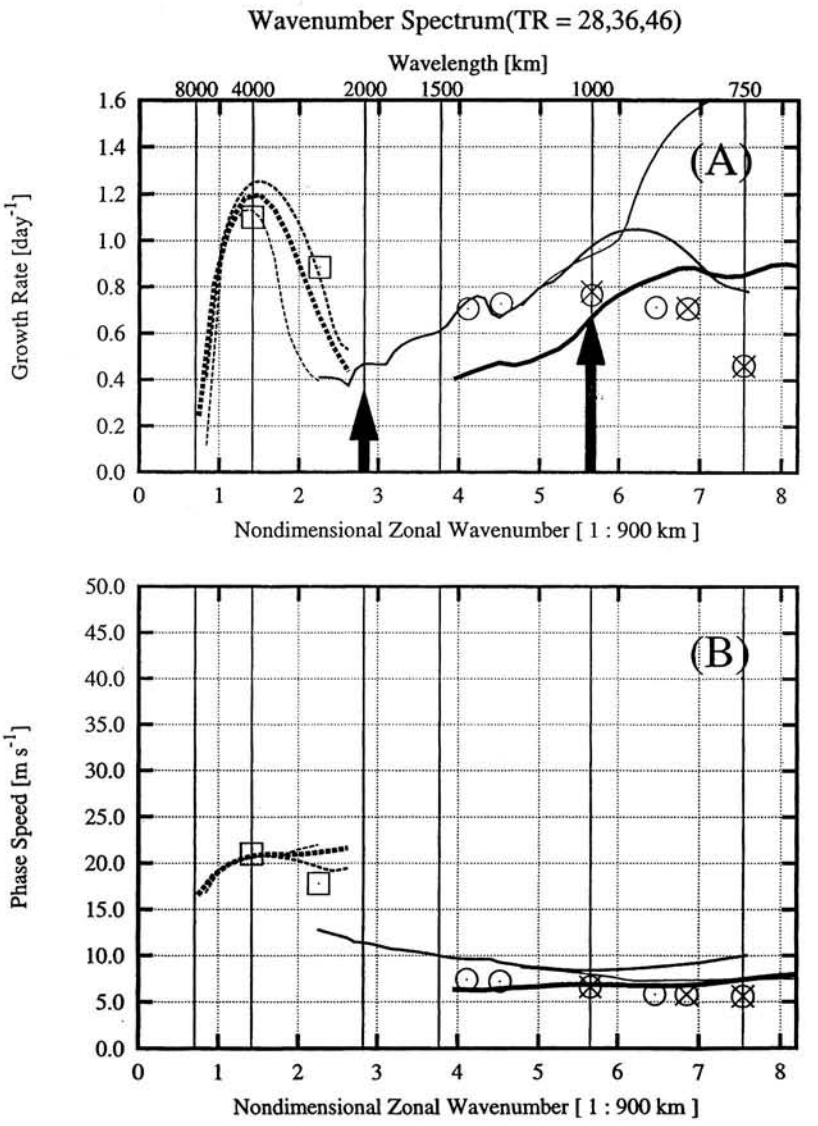

FIGURE 6 (a) Growth rate as a function of zonal wavenumber for the spectrum of instabilities supported by the analytical model meridional cross-section shown in Fig. 5a. (B) Phase speed spectrum for the same model. The open circles superimposed are growth rates and phase speeds determined from the early stages of the nonlinear DNS integrations for comparison. The parameter TR denotes the wave number truncation of the Galerkin expansions employed to represent the hydrodynamic pecturbations, the light to heavy weighted dashed and solid lines in the long wavelength and short wavelength regimes corresponding to TR = 28, 36, 46 respectively.

now very similar in form to a conventional Charney-Eady mode, it has a wavelength of only 2000 km, half that of this conventional synoptic scale disturbance. Clearly, there appears to exist a route to "deep development" that does not begin with linear instability on the Charney–Eady branch of synoptic scale instability but rather with the growth of a subsynoptic scale structure which later amplifies through an upscale cascade of energy supported by the pairing interaction. Of course if the initial frontal structure were sufficiently elongate zonally so as to support the Charney-Eady wave then this disturbance would appear immediately. In nature, however, such elongate frontal structures do not always exist and not all cyclones occur on scales as large as that of the fundamental Charney-Eady mode. The upscale cascade route to deep development revealed by the analyses discussed herein may be rather important to the understanding of cyclogenesis in such circumstances.

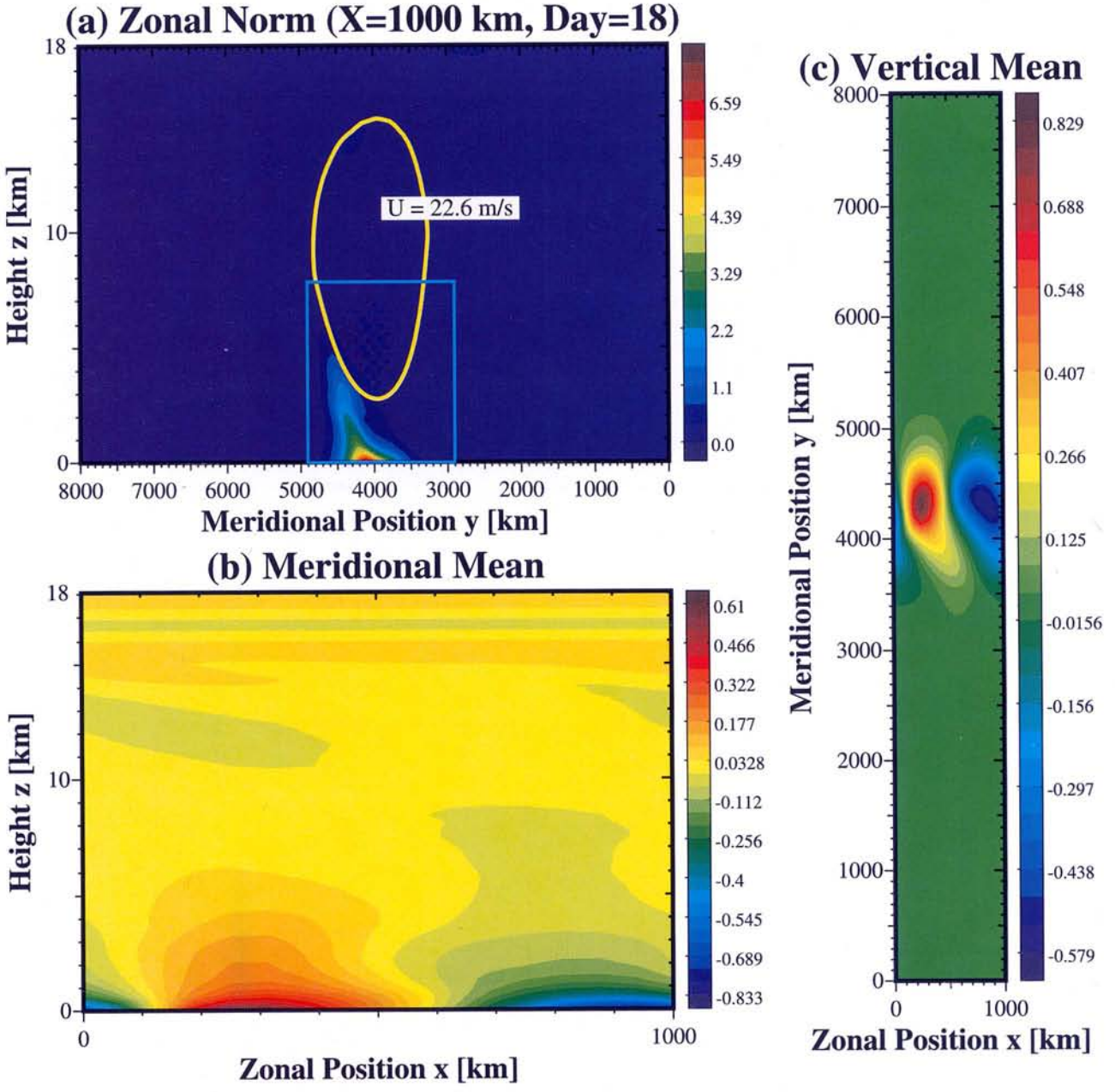

FIGURE 7 Structure of the fastest growing subsynoptic scale mode of baroclinic instability delivered by the initial value integration using the zonal mean state with structure shown in Fig. 5a. This subsynoptic scale structure is illustrated by (a) the zonal norm of the meridional velocity, (b) the meridional mean of the meridional velocity and (c) the vertical mean of the meridional velocity.

D. PAIRING IN VORTEX DYNAMICS ON THE SPHERE: ROSSBY-WAVE ARREST OF THE UPSCALE CASCADE AND THE "PARITY" OF GAS GIANT BANDS

One of the most compelling problems in planetary fluid dynamics, in which the upscale cascade of energy leads to the creation of coherent vortical structure that is observationally significant, is that concerning the origins of the latitudinally banded pattern of zonal velocity that characterizes the flow on the discs of the Gas Giant planets Jupiter, Saturn, Neptune and Uranus. Figure 11 illustrates this zonal wind structure for Jupiter based upon the analysis of the Voyager I and II observations by Beebe (1994), together with the fit to the data based

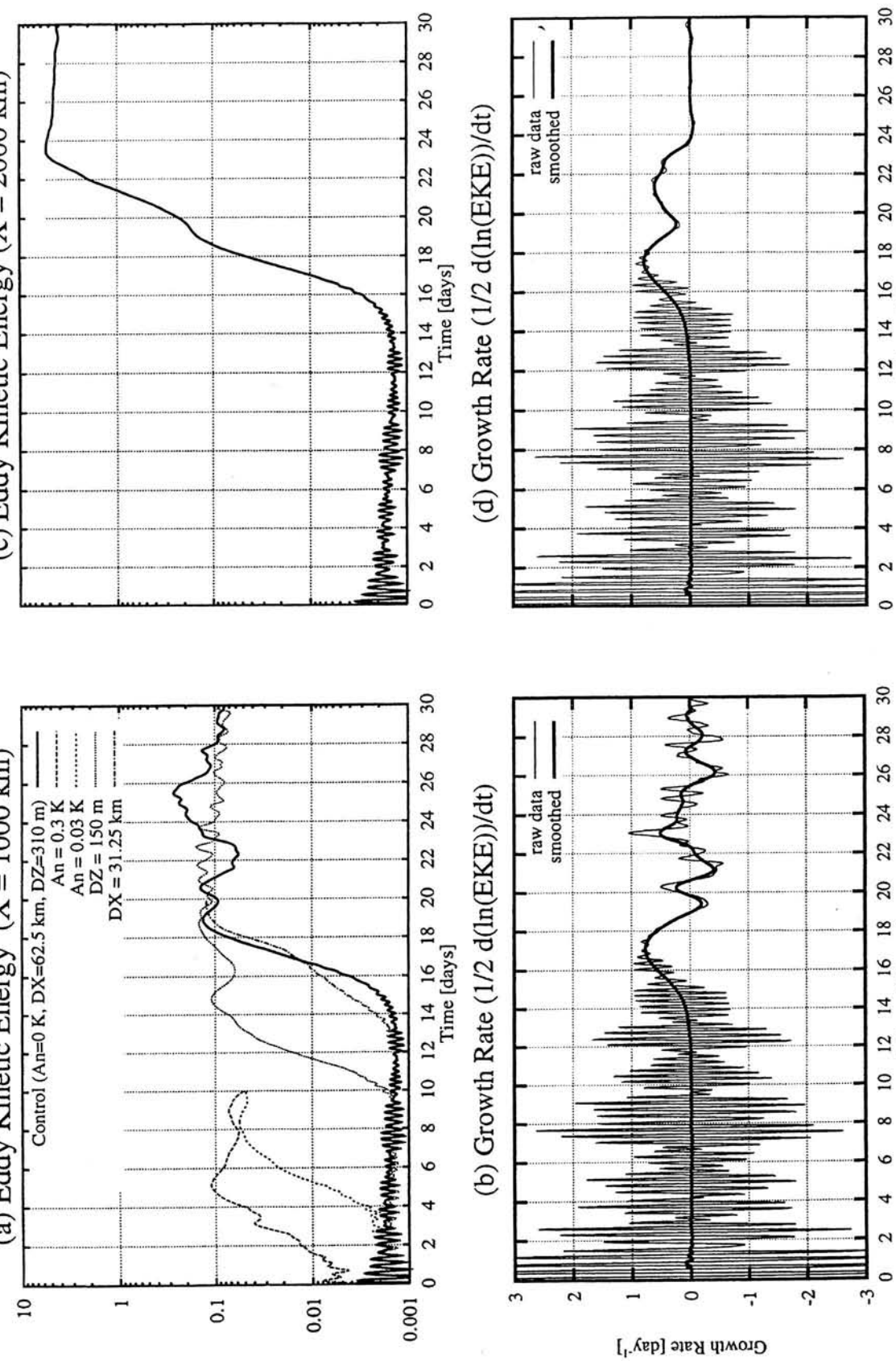

FIGURE 8 (a), (b) Kinetic energy and growth rate time series from the initial-value integrations of the nonlinear inelastic model when the zonal length of the domain is equal to 1000 km. (c), (d) same as (a), (b) but for the integration with domain length of 2000 km.

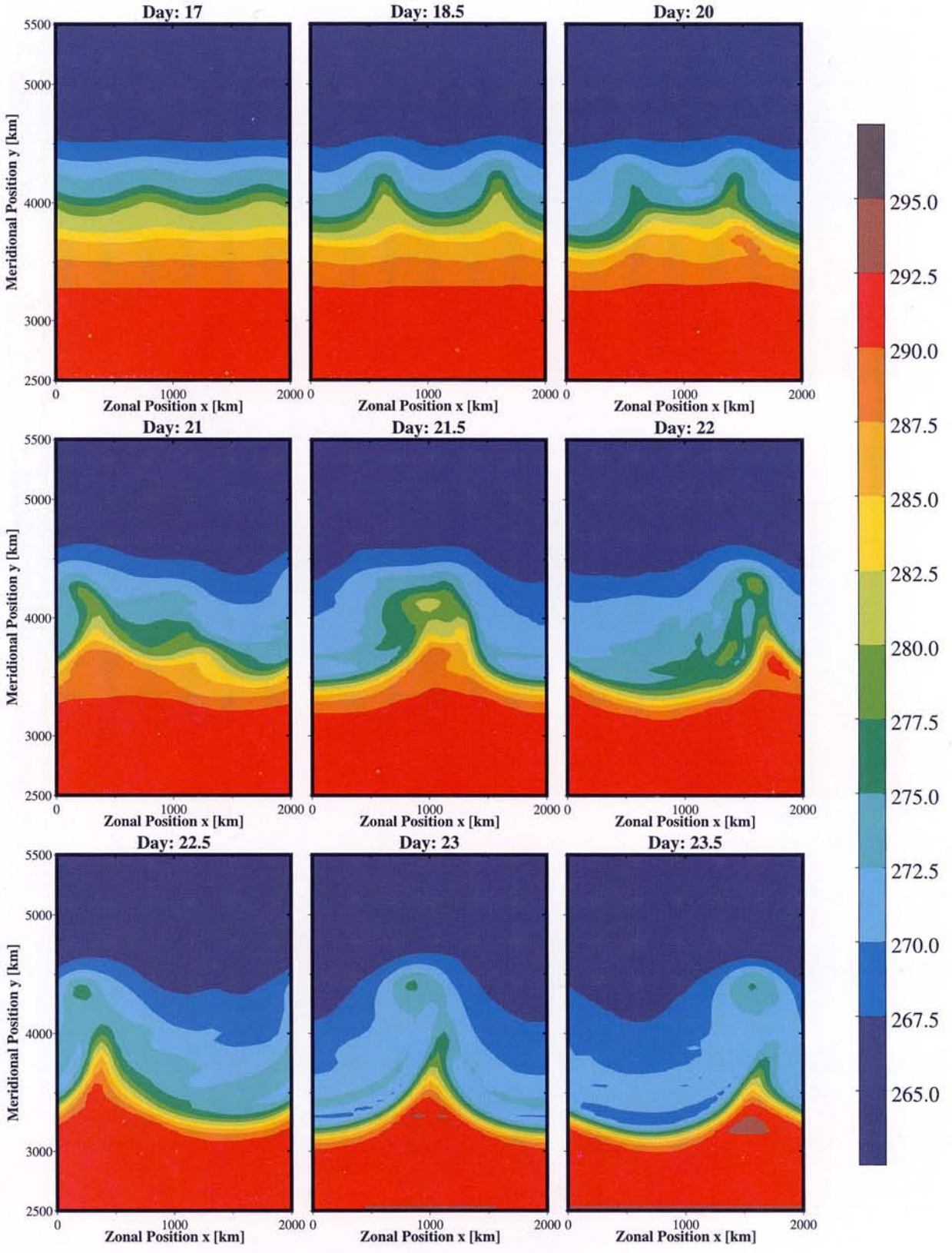

FIGURE 9 Surface potential temperature fields from the nonlinear time-dependent integration at a sequence of nine times in the evolution of the flow away from the parallel flow with meridional structure shown in Fig. 5a. Illustrates the pairing interaction.

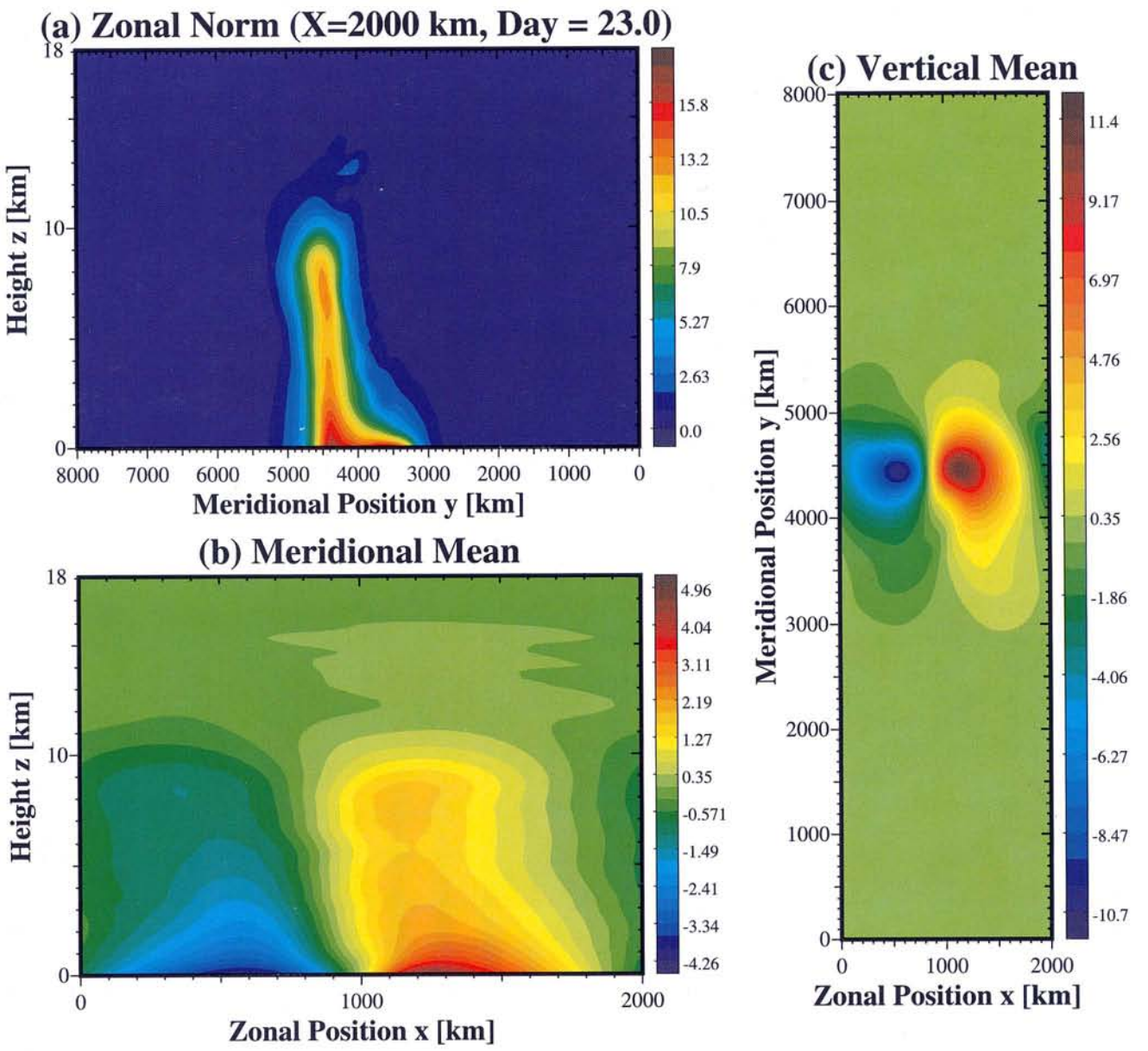

FIGURE 10 Same as Fig. 8 but for a time subsequent to completion of the pairing interaction.

upon the assumption that the flow corresponds to the pole-to-pole "staircase" in barotropic potential vorticity shown in Figure 11 (see Stuhne, 1999, for details of the construction procedure). Very recently, Cho and Polvani (1996) have demonstrated that some of the observed characteristics of these flows may be explained on the basis of simple unforced spherical shallow water integrations initialized with a "balanced" but otherwise random initial distribution of vorticity. The statistically stationary equilibrium states into which these flows evolve, when scaled to any one of the four Gas Giant planets, are banded in their zonal velocity patterns with the number of bands being approximately equal to the number observed on each of these objects. Although suggestive of the inevitability of the development of such banded structures, and of the utility of the shallow-water description of the flow in the "weather layer" on these planets, this explanation of the development of the bands that is embodied in such solutions of the unforced initial-value problem is significantly flawed.

In order to illustrate the nature of this flaw and to demonstrate that it is not due to any merely numerical

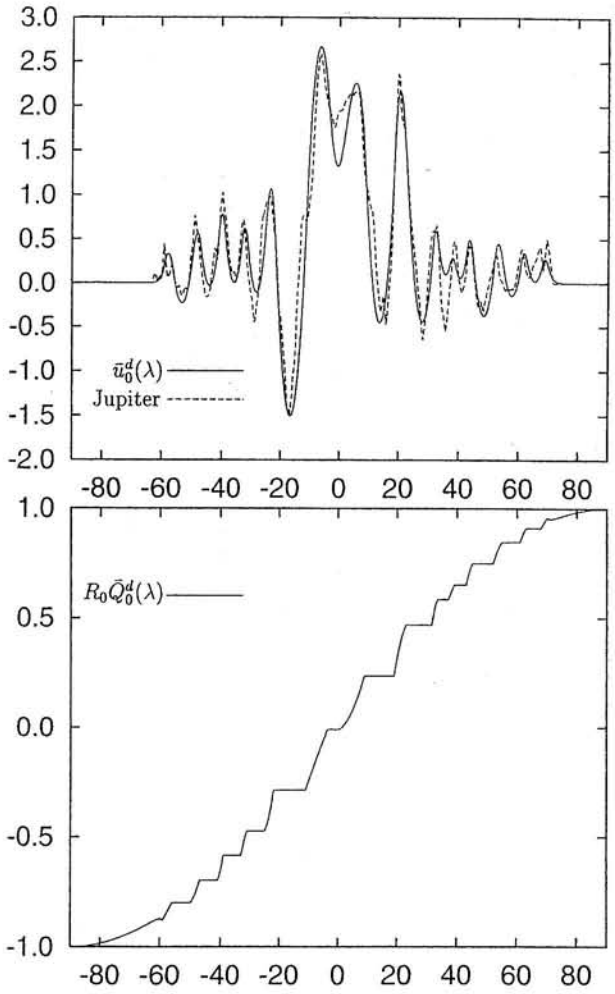

FIGURE 11 (Top) zonal velocity field as a function of latitude on the disc of Jupiter according to the analyses of Beebe (1994), compared to the zonal velocity field predicted by a model which assumes that barotropic potential vorticity varies over the disc according to the "monotonic staircase" model (bottom).

aspect of the shallow-water integrations reported by Cho and Polvani, it is useful to first reproduce their results using an entirely different numerical methodology. Whereas Cho and Polvani employed a shallow-water reduced form of the NCAR spectral model of the atmospheric general circulation as a basis for their numerical analyses, we have further tested the robustness of these results by employing the recently constructed shallow-water model of Stuhne and Peltier (1996, 1999), a model based upon regular icosahedral tiling of the sphere and the use of the multigrid method to evolve the shallow-water system of equations forward in time. With initial conditions corresponding to a random distribution of barotropic vorticity over the surface of the sphere, assumed to be in a state of Charney (1955) balance rather than in the state of higher-order balance assumed by Cho and Polvani (1996), Fig. 12 shows the results obtained for each of the Gas Giant planets when the shallow-water model is appropriately scaled to them, in terms of views of the vorticity field on their discs seen from a point in the equatorial plane. Inspection of these results demonstrates very clearly that in the initial phase of the evolution of these flows the dominant interaction that is occurring involves the same vortex-merging instability initially explored by McWilliams (1984), a pairing-driven interaction that leads to the coarsening of the vorticity distribution as kinetic energy cascades upscale, leading to the development of coherent vortical structures of ever-increasing size. Eventually, however, this vorticity-coarsening phase of flow evolution is arrested, evidently at the scale first discussed by Rhines (1975), beyond which Rossby-wave effects become important. After the vorticity distribution begins to relax into a field of Rossby waves, the latitudinally banded structure in zonal velocity begins to develop. Figure 13 compares the mean zonal flows obtained from the Gas Giant integrations using the icosahedral model with those previously obtained by Cho and Polvani (1996). Evident upon inspection of this figure is that these two independent sets of analyses are entirely consistent with one another, demonstrating that the statistical equilibrium zonal flows are not significantly influenced by the details of the shallow-water numerical model employed to obtain them.

This is important because it demonstrates that the flaw in these results, as possible explanations of the zonal flows on the discs of the Gas Giants, is not due to numerical abberation. The flaw in question has to do with the fact that, for each of the four planetary scales and rotation rates analysed, the sign of the equatorial jet in the statistical equilibrium state is retrograde rather than prograde, as is observed to be the case for the two largest Gas Giants, Jupiter and Saturn. The observed zonal flow on the disc of Jupiter was shown previously in Fig. 11. Detailed diagnostic analysis of the results of the new shallow-water integrations suggests an explanation as to why the specific mechanism of the arrest of the upscale turbulent cascade of kinetic energy that occurs in the unforced shallow-water model fails to predict the correct sign for the equatorial jets that dominate the flow in the weather layers of the two largest Gas Giant planets. The vorticity equation of the shallow-water dynamical model may be written as follows, in the form of a forced barotropic vorticity equation in which the forcing consists of the "unbalanced" component of the flow as:

$$\frac{\partial Q}{\partial t} + \mathbf{u}_b \cdot \nabla Q = \mathcal{F}(\theta,\lambda,t) \qquad (11)$$

in which Q is the barotropic potential vorticity, $\mathbf{u}_b$ is the

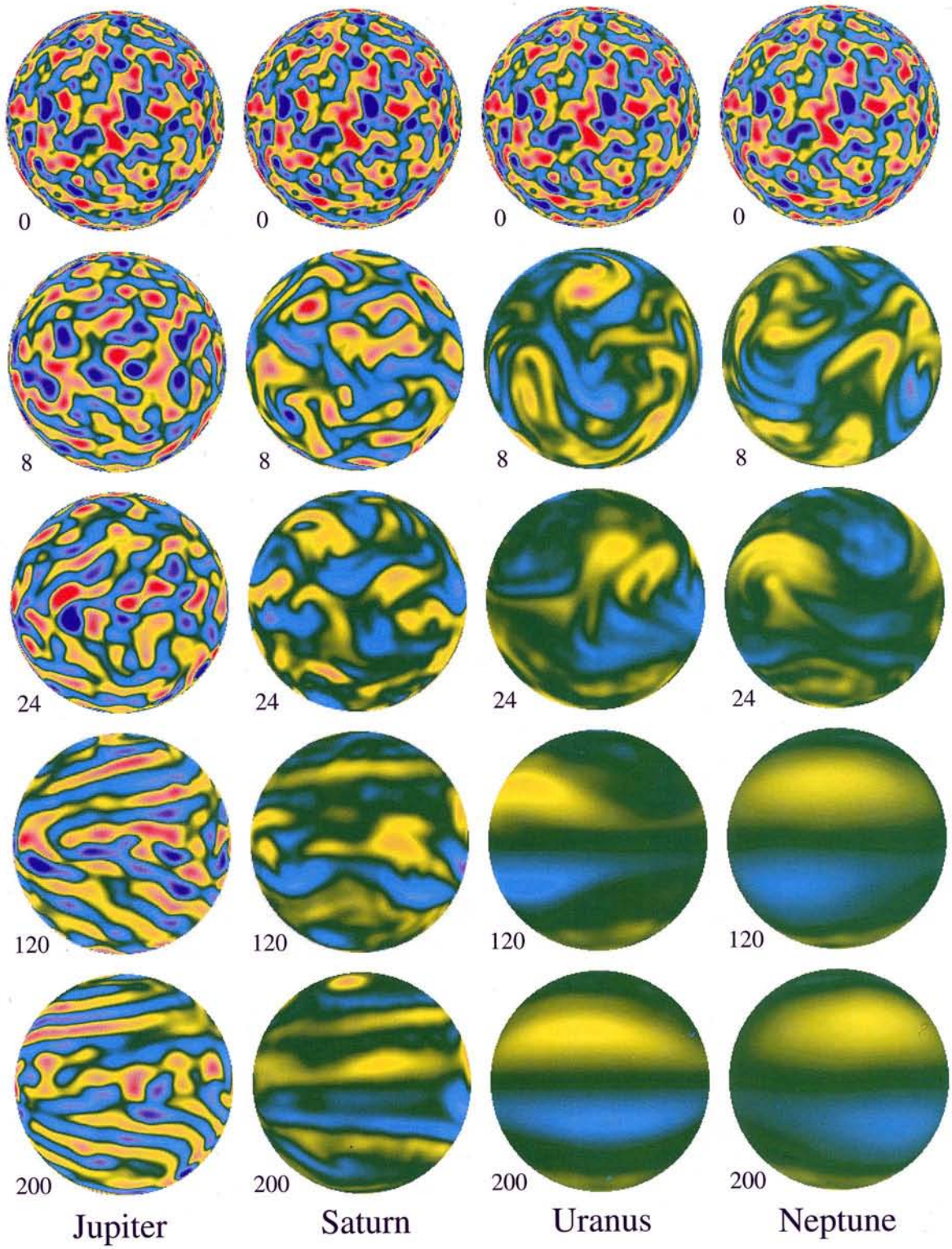

FIGURE 12 Evolution of the vorticity field delivered by freely evolving shallow-water integrations initialized with random but Charney (1959) balanced initial conditions. Results are shown for each of the Gas Giants with time measured in units of integral numbers of rotation periods shown adjacent to each image.

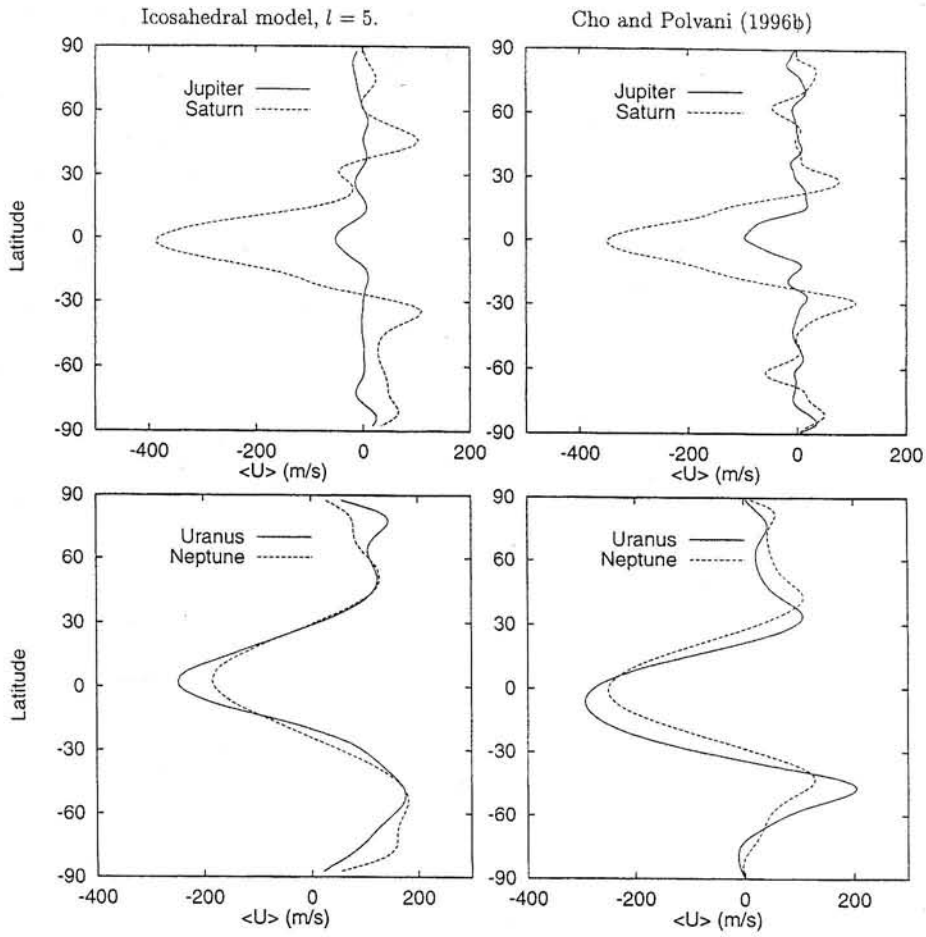

FIGURE 13 Statistical equilibrium zonal velocity fields from each of the four Gas Giant integrations performed using the new spherical icosahedral multigrid model compared with those previously obtained by Cho and Polvani (1996).

balanced (barotropic) component of the velocity field and $\mathcal{F}$ is the forcing of this balanced component by the evolving imbalance associated in part with surface gravity wave "activity". For the shallow-water model, the forcing associated with imbalance $\mathcal{F}$ has the specific form, with $\mathbf{u}_d$ the divergent component of the velocity field:

$$\mathcal{F}(\theta,\lambda,t) = -\nabla \cdot (\mathbf{u}_d\, Q) \tag{12}$$

with Q the barotropic PV field defined as

$$Q = = \nabla^2 \Psi + \mathrm{R}_o^{-1} \sin\theta \tag{13}$$

where the nondimensional parameter $\mathrm{R}_o = U/2\,\Omega_o \mathrm{r}_s$, r_s and Ω_o being the observable radius of the planet in question and angular velocity respectively and $U = \sqrt{2E_k}$ being a characteristic velocity taken to be the RMS velocity over the surface of the sphere. In Fig. 14 is shown the specific spatial structure over the sphere of the imbalance $\mathcal{F}$ at one instant of time, specifically after 200 planetary rotations, taken from the Jupiter integration. Inspection of these results demonstrates that the imbalance is of a form that will tend to "mix" the barotropic vorticity distribution most strongly in the equatorial region. That intense homogenization of barotropic PV near the equator will inevitably produce a retrograde equatorial jet is demonstrated in Fig. 15 which illustrates the fact that a staircase distribution of barotropic PV, a structure which appears to best fit all of the observed Gas Giant zonal flows, in which a broad "step" of uniform PV exists on the equator itself, must correspond to a retrograde zonal jet. Conversely, a PV staircase in which one of the PV discontinuities on the staircase is coincident with the equator corresponds to a zonal flow in which the equatorial jet is prograde. The zonal flow in Jupiter's weather layer (Fig. 11a) is somewhat more complex than either of these extremes as it appears to have a weak retrograde element on the equator which introduces a slight diminution of strength of what is otherwise an intense prograde equatorial jet. That even this minor feature is well captured

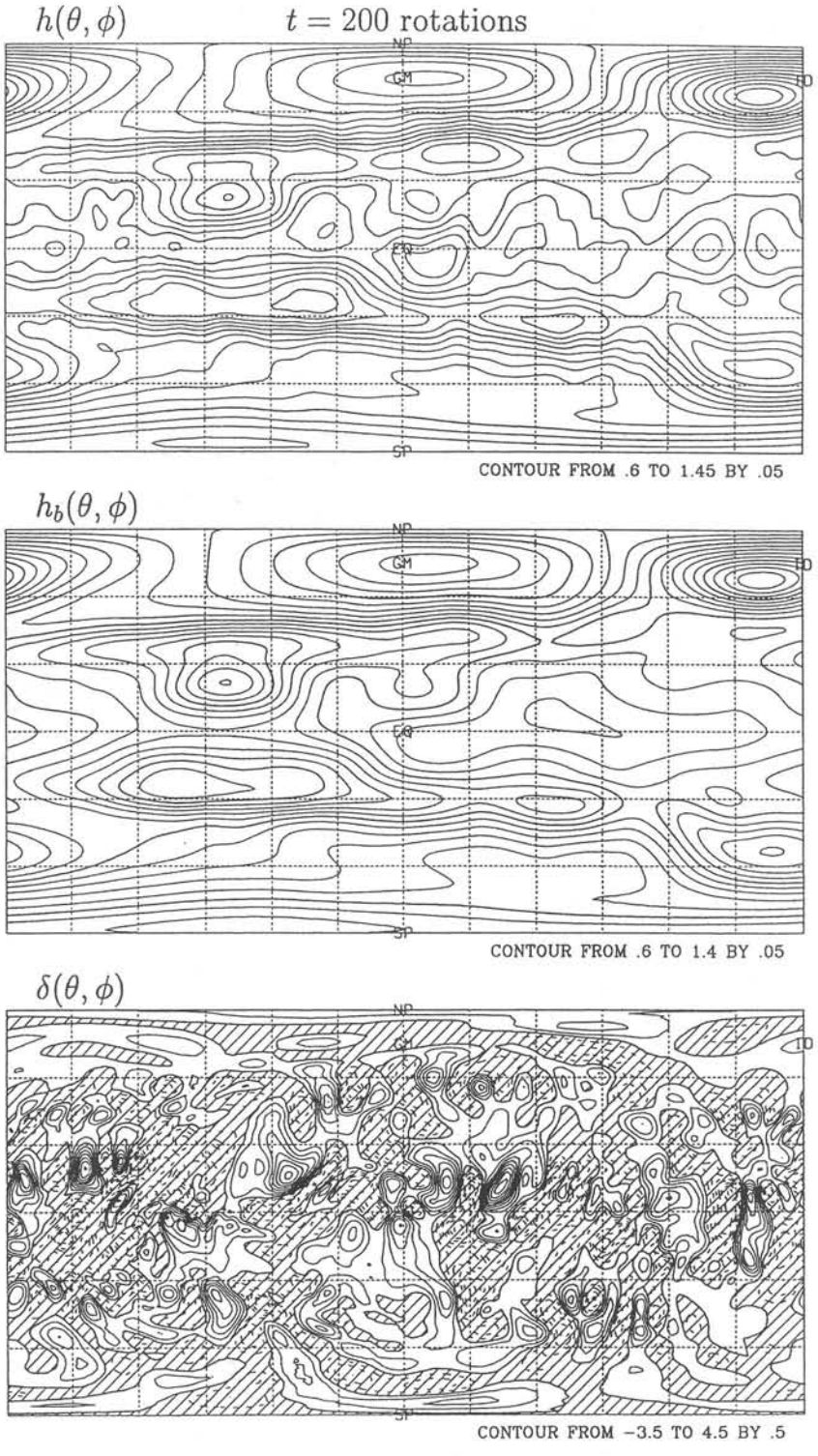

FIGURE 14 Three fields extracted from the shallow-water integration for a Jupiter scale object, respectively the height field h, the (Charney) balanced height field (h_b), and the divergence field δ (a measure of the imbalance in the model). These data correspond to a time 200 planetary rotations after initializing the flow with random (balanced) initial conditions in the vorticity field.

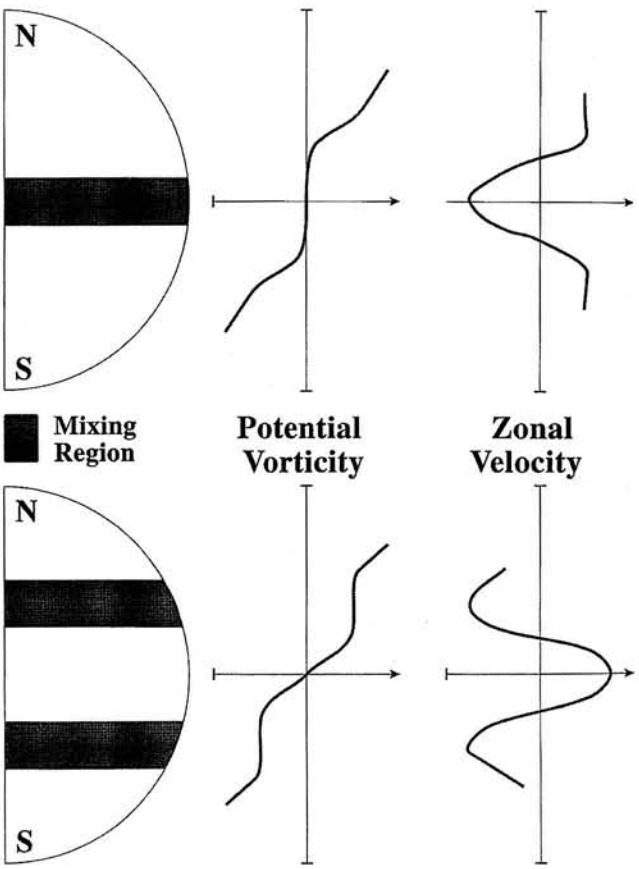

FIGURE 15 Sketch of the dependence of the sign of the equatorial jet in the balanced component of the flow as a function of the latitudinal regions over which the barotropic vorticity field is homogenized by mixing.

by our barotropic PV staircase construction of the latitudinal variation of zonal velocity is important. It is very well understood on theoretical grounds that such a monotonically increasing distribution of PV, from the south pole to the north pole across the disc, is finite-amplitude (Arnol'd, 1965, 1969) stable. This fact clearly explains, in principle, why the zonal flows observed by both Voyager I and II were essentially identical at large scale.

On the basis of the analysis described herein it should be clear that, although the unforced evolution of a shallow-water model from random vorticity initial conditions is successful in "explaining" the banded structure of the zonal flows observed on the discs of the Gas Giant planets, a model of this kind is unsuccessful in explaining what is arguably the most important characteristic of this zonal structure, namely the sign of atmospheric differential rotation in the equatorial region. In order to successfully predict this sign it is clear on the basis of the results described herein that the shallow-water model must be forced so as to homogenize barotropic potential vorticity in two primary zonal bands that are displaced from the equator itself, although some equatorial mixing is also required to explain the observed weakening of the prograde jet in this region. One simple mechanism through which strong forcing of the off-equatorial kind is quite likely to be realized is that which would naturally arise through the interaction of the thermal convection process in the convection zones of Jupiter and Saturn, which underlie the stably stratified weather layer in which the observed zonal flows develop, with the weather layer itself. If the convection process were to be organized into cells consisting of Taylor cyclinders aligned with the rotation axis, as envisioned by Busse (1994), then the outcropping of these convection cells in the off-equatorial region would be expected to effect precisely the spatial homogenization of the barotropic vorticity field in the off-equatorial region that is required to explain the dominantly prograde nature of the observed equatorial jets. Since the smaller Gas Giants may not be as convectively active in their interiors as are Jupiter and Saturn, this would also explain why their equatorial jets are retrograde, the unforced shallow-water model therefore providing an appropriate description of their zonal structures.

E. CONCLUSIONS

We have described three different hydrodynamic problems, each of which is of fundamental interest from an atmospheric dynamics perspective, in which the same upscale cascade of energy occurs as that which exerts such profound influence on fluid turbulence in flows restricted to two space dimensions. In each of these problems the flow either had access to all three space dimensions (Parallel shear flows, baroclinic zonal flow) or to 2.5 dimensions (shallow water flow on the sphere). The upscale cascade of energy that may occur in each of these circumstances involves the vortex-pairing interaction that is most clearly describable in the case of parallel shear flow and for which a detailed mathematical theory of the interaction exists which was presented in Section B. There it was shown that vortex merger could occur in principle by either one or the other of two different mechanisms of pairing, namely orbital merger and draining respectively. In parallel flows the mechanism of orbital merger dominates. Whether this interaction actually occurs in nature is strongly dependent upon the density stratification which in general acts so as to suppress this mechanism. In many naturally occurring flows, as opposed to those realized in the laboratory, fast-growing three-dimensional instabilities may induce intense three-dimensional turbulent mixing of the shear layer before the

pairing interaction can mature (e.g. see Caulfield and Peltier, 2000, for a detailed recent discussion of "the mixing transition" in stratified parallel flows).

In the discussion of the classical problem of baroclinic instability presented in Section C, we focused upon the fact that balanced baroclinic zonal flows containing weak cross-front gradients in potential vorticity may support subsynoptic scale modes of baroclinic instability with growth rates that are comparable to those of the classical Charney–Eady mode. So long as the flow in which a mode of this kind develops is constrained such that energy cannot cascade to longer zonal wavelength then disturbances of this kind should not (under dry atmospheric conditions) develop sufficiently so as to be important constituents of "weather". However, these waves are subject to a pairing interaction through which their energy level dramatically increases even when horizontal scale is restricted to be considerably less than the scale of maximum growth in the Charney-Eady branch. Yamasaki and Peltier (2001a,b) have recently suggested on this basis that there is a root to deep development that relies on precisely this upscale cascade scenario.

The final example of the upscale cascade discussed herein concerned the understanding of phenomenology arising in the integration of a shallow-water model in spherical geometry in the absence of forcing and from random balanced vorticity initial conditions. In such flows, so long as the initial vorticity distribution is characterized by vortices of dominant scale less than the Rhines scale, the flow initially evolves under the control of the same pairing-mediated upscale cascade of energy as that displayed so clearly in the two-dimensional Cartesian integrations of McWilliams (1984). This cascade is eventually arrested once the vorticity distribution begins to coarsen beyond the Rhines scale, the process of arrest being associated with the increasing influence of Rossby-wave activity. In unforced shallow-water integrations this mechanism of arrest delivers banded zonal flows of the kind observed on the discs of the Gas Giant planets. The equatorial jets in these banded zonal flows are, however, inevitably retrograde, whereas on the largest Gas Giants the equatorial jets are observed to be prograde. Analysis revealed that this flaw in the predicted zonal flows for the Gas Giants is due to the latitudinal distribution of mixing to which the barotropic vorticity field is subject in the unforced shallow-water integration due to the latitudinal distribution of imbalance. Based upon these results we were able to suggest a specific forcing mechanism which, when applied to the shallow-water model through an appropriate parameterization, should suffice to correct what is otherwise a fatal flaw in the shallow-water model of the discs of the largest of the Gas Giant planets. Results of such further analyses will be presented elsewhere.

References

Arnol'd, V. I., 1965: Conditions for nonlinear stability of stationary plane curvilinear flows of an ideal fluid. *Soviet Math.*, **6**, 773–777.

Arnol'd, V. I., 1969: On an a-priori estimate in the theory of hydrodynamic stability. *Am. Math. Soc. Trans.*, **79**, 267–275.

Baros, V. R. and A. Winn-Nielsen, 1974: On quasi-geostrophic turbulence: A numerical experiment. *J. Atmos. Sci.*, **31**, 609–621.

Beebe, R., 1994: Characteristic zonal winds and long lived vortices in the atmospheres of the outer planets, *Chaos*, **4**, 113–127.

Busse, F. H., 1994: A simple model of convection in the Jovian atmosphere, *Icarus*, **29**, 123–133.

Caulfield, C. and W. R. Peltier, 1994: Three dimensionalization of the stratified mixing layer. *Phys. Fluids*, **6**, 3803–3805.

Caulfield, C. and W. R. Peltier, 2000: The anatomy of the mixing transition in homogeneous and stratified parallel flows. *J. Fluid Mech.*, **43**, 1–47.

Charney, J. G., 1955: The use of the primivite equations in numerical prediction. *Tellus*, **7**, 22–35.

Charney, J. G., 1971: Geostrophic turbulence. *J. Atmos. Sci.*, **28**, 1087–1095.

Cho, Y.-K. and L. M. Polvani, 1996: The emergence of jets and vortices in freely evolving shallow water turbulence on the sphere. *Phys. Fluids*, **8**, 1531–1540.

Fjortoft, R., 1953: On the changes in the spectral distribution of kinetic energy for two dimensional non-divergent flow. *Tellus*, **5**, 225–230.

Hua, B. L. and D. B. Haidvogel, 1986: Numerical simulations of the vertical structure of quasi-geostrophic turbulence. *J. Atmos. Sci.*, **43**, 2923–2936.

Kelley, R. E., 1967: On the stability of an inviscid shear layer which is periodic in space and time. *J. Fluid Mech.*, **27**, 657–689.

Klaassen, G. P. and W. R. Peltier, 1985: The onset of turbulence in finite amplitude Kelvin–Helmholtz billows. *J. Fluid Mech.*, **155**, 1–35.

Klaassen, G. P. and W. R. Peltier, 1989: The role of transverse instabilities in the evolution of free shear layers, *J. Fluid Mech.*, **202**, 367–402.

Klaassen, G. P. and W. R. Peltier, 1991: The influence of stratification on secondary instability in free shear layers, *J. Fluid Mech.*, **227**, 71–106.

Kolmogorov, A. N., 1941: The local structure of turbulence in incompressible viscous fluid over very large Reynolds numbers, and dissipation of energy in the locally isotropic turbulence. (English translation: *Proc. R. Soc. Lon. A434*, Turbulence and Stochastic Processes: Kolmogorov's Ideas, 50 Years On, pp. 9–17.)

Lambert, S. J., 1981: A diagnostic study of global energy and enstrophy fluxes and spectra, *Tellus*, **33**, 411–414.

Maltrud, M. E. and G. K. Vallis, 1991: Energy spectra and coherent structures in forced two-dimensional and beta-plane turbulence, *J. Fluid Mech.*, **228**, 321–342.

McWilliams, J. C., 1984: The emergence of isolated coherent vortices in turbulent flow, *J. Fluid Mech.*, **146**, 21–43.

Pierrehumbert, R. T. and S. E. Widnall, 1982: The two and three dimensional instabilities of a spatially periodic shear layer, *J. Fluid Mech.*, **114**, 59–82.

Potylitsin, P. G. and W. R. Peltier, 1998: Stratification effects on the stability of columnar vortices on the f-plane, *J. Fluid Mech.*, **355**, 45–79.

Potylitsin, P. G. and W. R. Peltier, 1999: Three dimensional destabilization of Stuart vortices: the influence of rotation and ellipticity, *J. Fluid Mech.*, **387**, 205–226.

Rhines, P. B., 1975: Waves and turbulence on a β-plane, *J. Fluid Mech.*, **69**, 417–443.

Salmon, R., 1998: *Lectures on Geophysical Fluid Dynamics*, Oxford University Press.

Smyth, W. D. and W. R. Peltier, 1990: Three dimensional primary instabilities of a stratified, dissipative, parallel flow. *Geophys. Astrophys. Fluid Dynam.*, **52**, 249–261.

Smyth, W. D. and W. R. Peltier, 1991: Instability and transition in finite amplitude Kelvin–Helmholtz and Homboe waves, *J. Fluid Mech.*, **228**, 387–415.

Smyth, W. D. and W. R. Peltier, 1993: Two dimensional turbulence in homogeneous and stratified shear layers, *Geophys. Astrophys. Fluid Dynam.*, **69**, 1–32.

Smyth, W. D. and W. R. Peltier, 1994: Three dimensionalization of barotropic vortices on the f-plane, *J. Fluid Mech.*, **265**, 25–64.

Stuart, J. T., 1967: On finite amplitude oscillations in laminar mixing layers, *J. Fluid Mech.*, **29**, 417–440.

Stuhne, G. R., 1999: Classical hydrodynamics on the sphere: Gas giant phenomenology and novel numerical methodology. Ph.D. Dissertation, Department of Physics, University of Toronto.

Stuhne, G. R. and W. R. Peltier, 1996: Vortex erosion and amalgamation in a new model of large scale flow on the sphere, *J. Comput. Phys.*, **121**, 58–81.

Stuhne, G. R. and W. R. Peltier, 1999: New icosahedral grid-point discretizations of the shallow water equations on the sphere. *J. Comput. Phys.*, **148**, 23–55.

Yamasaki, Y. H. and W. R. Peltier, 2001a: On the existence of subsynoptic scale baroclinic instability and the nonlinear evolution of shallow disturbances, *J. Atmos. Sci.*, **58**, 657–683.

Yamasaki, Y. H. and W. R. Peltier, 2001b: Baroclinic instability in an Euler equations based column model: the coexistence of a deep synoptic scale mode and a shallow subsynoptic scale mode, *J. Atmos, Sci.*, **58**, 780–792.